Beyond Flory theory: Distribution functions for interacting lattice trees

Angelo Rosa[*]

SISSA-Scuola Internazionale Superiore di Studi Avanzati, Via Bonomea 265, 34136 Trieste, Italy

Ralf Everaers[†]

Univ Lyon, Ens de Lyon, Univ Claude Bernard Lyon 1, CNRS, Laboratoire de Physique and Centre Blaise Pascal, F-69342 Lyon, France
(Received 14 October 2016; published 12 January 2017)

While Flory theories [J. Isaacson and T. C. Lubensky, J. Physique Lett. **41**, 469 (1980); M. Daoud and J. F. Joanny, J. Physique **42**, 1359 (1981); A. M. Gutin *et al.*, Macromolecules **26**, 1293 (1993)] provide an extremely useful framework for understanding the behavior of interacting, randomly branching polymers, the approach is inherently limited. Here we use a combination of scaling arguments and computer simulations to go beyond a Gaussian description. We analyze distribution functions for a wide variety of quantities characterizing the tree connectivities and conformations for the four different statistical ensembles, which we have studied numerically in [A. Rosa and R. Everaers, J. Phys. A: Math. Theor. **49**, 345001 (2016) and J. Chem. Phys. **145**, 164906 (2016)]: (a) ideal randomly branching polymers, (b) $2d$ and $3d$ melts of interacting randomly branching polymers, (c) $3d$ self-avoiding trees with annealed connectivity, and (d) $3d$ self-avoiding trees with quenched ideal connectivity. In particular, we investigate the distributions (i) $p_N(n)$ of the weight, n, of branches cut from trees of mass N by severing randomly chosen bonds; (ii) $p_N(l)$ of the contour distances, l, between monomers; (iii) $p_N(\vec{r})$ of spatial distances, $\vec{r}$, between monomers, and (iv) $p_N(\vec{r}|l)$ of the end-to-end distance of paths of length l. Data for different tree sizes superimpose, when expressed as functions of suitably rescaled observables $\vec{x} = \vec{r}/\sqrt{\langle r^2(N)\rangle}$ or $x = l/\langle l(N)\rangle$. In particular, we observe a generalized Kramers relation for the branch weight distributions (i) and find that all the other distributions (ii–iv) are of Redner-des Cloizeaux type, $q(\vec{x}) = C\,|x|^\theta\,\exp\left(-(K|x|)^t\right)$. We propose a coherent framework, including generalized Fisher-Pincus relations, relating most of the RdC exponents to each other and to the contact and Flory exponents for interacting trees.

I. INTRODUCTION

A randomly branched tree is a finite connected set of bonds that contain no closed loops and which is embedded in a d dimensional space. Aside from their importance in statistical physics [1] and the intriguing connection to relevant physical problems such as percolation [2], randomly branched trees have received particular attention for being practically implicated in the modeling of branched [3], ring [4–10], and supercoiled [11] polymers.

As customary in polymer physics [3,12], the behavior of randomly branched trees can be analyzed in terms of a small set of exponents describing how expectation values for observables characterizing tree connectivities and conformations vary with the weight, N, of the trees or the contour distance, L, between nodes:

$$\langle N_{\text{br}}(N)\rangle \sim N^\epsilon, \tag{1}$$

$$\langle L(N)\rangle \sim N^\rho, \tag{2}$$

$$\langle R^2(L)\rangle \sim L^{2\nu_{\text{path}}}, \tag{3}$$

$$\langle R_g^2(N)\rangle \sim N^{2\nu}, \tag{4}$$

$$\langle N_c(N)\rangle \sim N^{\gamma_c}, \tag{5}$$

$$\langle N_c^{\text{inter}}(N)\rangle \sim N^\beta. \tag{6}$$

Here, $\langle N_{\text{br}}(N)\rangle$ denotes the average branch weight; $\langle L(N)\rangle$ the average contour distance or length of paths on the tree;

$\langle R^2(L)\rangle$ the mean-square spatial distance between nodes with fixed contour distance; $\langle R_g^2(N)\rangle$ the mean-square gyration radius of the trees; $\langle N_c(N)\rangle$ the average number of intratree pair contacts; $\langle N_c^{\text{inter}}(N)\rangle$ the average number of pair contacts between different trees in melt. By construction, $\nu = \rho\,\nu_{\text{path}}$, and the relation $\epsilon = \rho$ is expected to hold in general [13].

Exact values for the exponents are known only for a very few number of cases. For ideal noninteracting trees, the exponents $\rho^{\text{ideal}} = \epsilon^{\text{ideal}} = \nu_{\text{path}}^{\text{ideal}} = 1/2$ and $\nu^{\text{ideal}} = 1/4$ [14,15]. Furthermore, $\gamma_c^{\text{ideal}} = 2 - d\nu^{\text{ideal}}$ where d denotes the dimension of the embedding space. For interacting trees, the only known exact result [16] is the value $\nu = 1/2$ for self-avoiding trees in $d = 3$. On the other hand, numerical results [13,17–19] as well as approximate theoretical calculations [20,21] confirm that Flory theories [8,22–25] provide a useful framework for discussing the *average* behavior, Eqs. (1) to (4), of a wide range of interacting tree systems. While being remarkably successful though, due to its simplicity Flory theory is inevitably affected by serious known shortcomings and limitations [26,27]. They are, for instance, manifest in (small) deviations of predicted from observed or exactly known values for exponents as those defined in Eqs. (1) to (5), and, importantly, it does not give any insight for the equally relevant exponent β, Eq. (6). In the case of linear chains, these limitations are much more pronounced in the distribution functions for the corresponding observables, which contain a wealth of additional information.

Little seems to be known about the even larger range of configurational distribution functions for interacting trees. In the following, we present numerical results based on a detailed analysis of five different tree ensembles, which we

[*]anrosa@sissa.it

[†]ralf.everaers@ens-lyon.fr

have simulated in Refs. [18,19]: (i) ideal randomly branching polymers, (ii) $2d$ and $3d$ melts of interacting randomly branching polymers, (iii) $3d$ self-avoiding trees with annealed connectivity, and (iv) $3d$ self-avoiding trees with quenched ideal connectivity. We analyze the distributions along the lines of known relations for ideal trees and linear chains and propose a coherent framework, including generalized Fisher-Pincus relations, relating most of the exponents characterizing the distribution functions to each other and to the contact and Flory exponents for interacting trees.

The paper is organized as follows: In Sec. II we briefly summarize the theoretical background and list a number of useful results for ideal and interacting linear chains and trees. In Sec. III we give a few details on the numerical methodologies employed for simulating the trees and analyzing their connectivity. Finally, we present and discuss our results in Sec. IV and briefly conclude in Sec. V.

II. THEORETICAL BACKGROUND

A. Ideal trees

Consider a tree of mass N defined as $N + 1$ monomers connected by N bonds or Kuhn segments. For ideal trees, Daoud and Joanny [23] calculated the partition function $\mathcal{Z}_N$ in the continuum approximation:

$$\mathcal{Z}_N = \frac{I_1(2\lambda N)}{\lambda N} \simeq \begin{cases} \frac{e^{2\lambda N}}{2\pi^{1/2}(\lambda N)^{3/2}}, & \lambda N \gg 1 \\ 1 + \frac{(\lambda N)^2}{2}, & \lambda N \ll 1 \end{cases}, \quad (7)$$

where $I_1(x)$ is the first modified Bessel function of the first kind, λ the branching fugacity, and $\mathcal{Z}_0 = 1$. Removing a randomly chosen bond splits a branch of size $n < N/2$ from the remaining tree of size $N - n - 1$. For ideal trees, the probability distribution, $p_N(n)$, of branch sizes is given by the Kramers theorem [3],

$$p_N(n) = \frac{\mathcal{Z}_n \mathcal{Z}_{N-1-n}}{\sum_{n=0}^{N-1} \mathcal{Z}_n \mathcal{Z}_{N-1-n}}, \quad (8)$$

and related to sum over all possible ways of splitting the tree. From this expression, it is possible to derive the following asymptotic relations:

$$p_N(n) \simeq \begin{cases} \frac{\lambda (\lambda N)^{3/2}}{4\pi^{1/2}(\lambda n)^{3/2}(\lambda(N-n))^{3/2}}, & \lambda n \gg 1 \\ \frac{\lambda}{4\pi^{1/2}(\lambda n)^{3/2}}, & \lambda N \gg \lambda n \gg 1 \\ \frac{1}{N}, & \lambda N \ll 1 \end{cases}, \quad (9)$$

with $\langle N_{\mathrm{br}}(N) \rangle \sim N^{1/2} \equiv N^{2-x}$, where $x = 3/2$ is the scaling exponent describing the decay of $p_N(n)$ in the large-N limit, Eq. (9).

B. Flory theory of interacting trees

Flory theories are formulated as a balance of an entropic elastic term and an interaction energy [28]:

$$\mathcal{F} = \mathcal{F}_{\mathrm{el}}(N,R) + \mathcal{F}_{\mathrm{inter}}(N,R). \quad (10)$$

In the standard case of self-avoiding walks, $\frac{\mathcal{F}_{\mathrm{el}}(N,R)}{k_B T} \sim \frac{R^2}{l_K^2 N}$ represents the entropic elasticity of a linear chain, while $\frac{\mathcal{F}_{\mathrm{inter}}(N,R)}{k_B T} \sim v_2 \frac{N^2}{R^d}$ represents the two-body repulsion between

segments, which dominates in good solvent. For interacting trees, the elastic free energy takes the form [24]

$$\frac{\mathcal{F}_{el}}{k_B T} \sim \frac{R^2}{l_K L} + \frac{L^2}{N l_K^2}. \quad (11)$$

The expression reduces to the entropic elasticity of a linear chain for unbranched trees with quenched $L = l_K N$. The first term of Eq. (11) is the usual elastic energy contribution for stretching a polymer of linear contour length L at its ends [24]. The second term penalizes deviations from the ideal branching statistics, which lead to longer paths and hence spatially more extended trees. More formally, it is calculated from the partition function of an ideal branched polymer of N bonds with L bonds between two arbitrary fixed ends [15,24,29]. For trees with quenched connectivity, Eq. (11) has to be evaluated for the given mean path length L and then minimized with respect to R. For trees with annealed connectivity, Eq. (11) needs to be minimized with respect to both R and L.

In this form, the theory predicts values for the exponents ν, ρ, and ν_{path} for a wide range of tree systems [18,19,25] as a function of the embedding dimension, d, as well as relations between these exponents. For example, optimizing L for annealed trees for a *given* asymptotic, $R \sim N^\nu$, yields

$$\rho = \frac{1 + 2\nu}{3}, \quad (12)$$

$$\nu_{\mathrm{path}} = \frac{3\nu}{1 + 2\nu}, \quad (13)$$

independently of the type of volume interactions causing the swelling in the first place. Plausibly, a fully extended system, $\nu = 1$, is predicted not to branch, $\rho = 1$, and to have a fully stretched stem, $\nu_{\mathrm{path}} = \nu = 1$. For the radius of ideal randomly branched polymers, $\nu = 1/4$, one recovers $\rho = 1/2$ and Gaussian path statistics, $\nu_{\mathrm{path}} = 1/2$.

C. Linear chains beyond Flory theory

In spite of its simplicity, the Flory theory is undoubtedly accurate. Yet—and even for linear polymers—there is more than can be described by means of Flory theory. Let us take, for instance, the number of self-avoiding walks, which is given by Refs. [27,30],

$$\mathcal{Z}_{\mathrm{SAW}}(N) \sim \mu^N N^{\gamma - 1}, \quad (14)$$

with a universal exponent γ and a nonuniversal constant μ characteristic of the employed lattice. Flory theory can neither predict the functional form of Eq. (14), nor the numerical value of γ [31], nor the related contact probability [27],

$$p_c \sim N^{-\nu(d+\theta)}, \quad (15)$$

$$\theta = \frac{\gamma - 1}{\nu}. \quad (16)$$

Furthermore, Flory theory incorrectly predicts that stretched chains exhibit essentially Gaussian behavior with volume interactions becoming quickly negligible. Instead, the end-to-end distance distribution of self-avoiding walks is to

an excellent approximation [32] given by the Redner-des Cloizeaux (RdC) [27,33] distribution,

$$p_N(\vec{r}) = \frac{1}{\langle R^2(N)\rangle^{d/2}} \, q\left[\frac{\vec{r}}{\sqrt{\langle R^2(N)\rangle}}\right], \qquad (17)$$

$$q(\vec{x}) = C\,x^\theta\,\exp[-(Kx)^t], \qquad (18)$$

with $q(\vec{x})$ independent of N. For small distances, Eq. (18) is dominated by the power law with the exponent θ given by the contact exponent Eq. (15). For large distances, the chain behaves like a string of N/g blobs of size $\xi \sim g^\nu$. For a given extension r/ξ, the free energy of k_BT per blob implies that the exponents t is given by [34,35]

$$t = \frac{1}{1-\nu}. \qquad (19)$$

Interestingly, knowledge of the two exponents is sufficient to reconstruct the entire distribution function, because the constants C and K are determined by the conditions (1) that the distribution is normalized ($\int q(\vec{x})d\vec{x} \equiv 1$) and (2) that the second moment was chosen as the scaling length ($\int |x|^2 q(\vec{x})d\vec{x} \equiv 1$):

$$C = t\,\frac{\Gamma\left(1+\frac{d}{2}\right)\Gamma^{\frac{d+\theta}{2}}\left(\frac{2+d+\theta}{t}\right)}{d\,\pi^{d/2}\,\Gamma^{\frac{2+d+\theta}{2}}\left(\frac{d+\theta}{t}\right)}, \qquad (20)$$

$$K^2 = \frac{\Gamma\left(\frac{2+d+\theta}{t}\right)}{\Gamma\left(\frac{d+\theta}{t}\right)}. \qquad (21)$$

III. MODEL AND METHODS

In this section, we account very briefly for the algorithms used for generating equilibrated configurations of trees (Sec. III A) and the numerical schemes employed for their analysis (Sec. III B). The reader interested in more technical details may look into our former works [18,19]. A longer discussion is dedicated to how we extracted and extrapolated scaling exponents for RdC functions and contacts (Sec. III C). Quantitative details as well as tabulated values for single-tree statistics are presented in the Appendix.

A. Generation of equilibrated tree configurations for different ensembles

To simulate randomly branching polymers with *annealed* connectivity, we employ a slightly modified version of the "amoeba" Monte Carlo algorithm [36] for trees on the cubic lattice with periodic boundary conditions. In the model, connected nodes occupy adjacent lattice sites. As there is no bending energy term, the lattice constant equals the Kuhn length, l_K, of linear paths across ideal trees. The functionality of nodes is restricted to the values $f = 1$ (a leaf or branch tip), $f = 2$ (linear chain section), and $f = 3$ (branch point). We have studied ideal noninteracting trees, $3d$ self-avoiding trees, and $2d$ and $3d$ melts of trees.

In addition, we have studied randomly branched trees with *quenched ideal* connectivity. For this ensemble, we have resorted to an equivalent off-lattice bead-spring model and studied it via molecular dynamics simulations. In this model, trees are represented by the same number of degrees

of freedom, with bonds described as harmonic springs of average length equal to l_K. This allows a one-to-one mapping to and from the lattice model. Furthermore, beads interact with a repulsive soft potential whose strength is tuned in such a way that the gyration radii of self-avoiding lattice trees remain invariant under the switch to the off-lattice model, if their quenched connectivities are drawn from the ensemble of self-avoiding on-lattice trees with annealed connectivity.

For all our ensembles, the tree sizes are $3 \leqslant N \leqslant 1800$ for ideal and self-avoiding trees [18] and $3 \leqslant N \leqslant 900$ for melts of trees [19].

B. Analysis of tree connectivity

We have analyzed tree connectivities using a variant of the "burning" algorithm for percolation clusters [37,38]. The algorithm works iteratively: each step consists in removing from the list of all nodes the ones with functionality $= 1$ and updating the functionalities and the indices of the remaining ones accordingly. The algorithm stops when only one node (the "center" of the tree) remains in the list. In this way, by keeping track of the nodes that have been removed it is possible to obtain information about the mass and shape of branches. The algorithm can be then generalized to detect the minimal path length $l_{i,j}$ between any pair of nodes i and j: it is in fact sufficient that both nodes "survive" the burning process.

C. Finite-size effects

As discussed in detail in our former works [18,19], extrapolation to the large-N limit of scaling exponents is a delicate issue. In general, in fact, our data are affected by finite-size effects and extracted exponents are either (i) effective (crossover) exponents valid for the particular systems and system sizes we have studied or (ii) *estimates* of true, asymptotic exponents, which suffer from uncertainties related to the extrapolation to the asymptotic limit.

1. Extrapolating scaling exponents of distribution functions

Pairs of exponents (θ_l, t_l), $(\theta_{\text{path}}, t_{\text{path}})$, and $(\theta_{\text{tree}}, t_{\text{tree}})$ are obtained by best fits of data for distribution functions $p_N(l)$, $p_N(\vec{r}|l)$, and $p_N(\vec{r})$ to the corresponding two-parameter Redner-des Cloizeaux functions [Eqs. (26), (32), and (35), respectively]. As shown in Tables II–IV, the values obtained from these fits display nonnegligible finite-size effects. Then, the search for extrapolated values has required two separate strategies.

For exponents (θ_l, t_l) and $(\theta_{\text{tree}}, t_{\text{tree}})$, we follow a procedure similar to the one outlined first in Ref. [13] and adopted later by us in Refs. [18,19]. It combines together the two following extrapolation schemes:

(1) A fit of the data for θ_l and θ_{tree} to the following three-parameter fit functions:

$$\log\theta_l = a + bN^{-\Delta_0} - b(\Delta - \Delta_0)N^{-\Delta_0}\log N$$
$$\equiv a + be^{-\Delta_0\log N} - b(\Delta - \Delta_0)e^{-\Delta_0\log N}\log N \quad (22)$$

and

$$\theta_{\text{tree}} = a + bN^{-\Delta_0} - b(\Delta - \Delta_0)N^{-\Delta_0}\log N$$
$$\equiv a + be^{-\Delta_0\log N} - b(\Delta - \Delta_0)e^{-\Delta_0\log N}\log N \quad (23)$$

and analogous expressions for t_l and t_{tree}. Equations (22) and (23) correspond to a self-consistent linearization of the three-parameter fit $\theta_{l,\text{tree}} = a + b\frac{1}{N^{\Delta}}$ around $\Delta = \Delta_0$. We have carried out a one-dimensional search for the value of Δ_0 for which the fits yield vanishing $N^{-\Delta_0} \log N$ term. Note that we have analyzed data for θ_l (and t_l) in Eq. (22) in the form "log θ_l versus log N" (log-log), while for θ_{tree} (and t_{tree}) we have used in Eq. (23) data in a log-linear representation, "θ_{tree} versus log N." These two different functional forms have been found to produce the best (statistical significant) fits.

(2) In the second method we fixed $\Delta = 1$, and we calculated the corresponding two-parameter best fits to the same data.

Results from the two fits are summarized separately in Tables II and IV and their averages taken for our final estimates of scaling exponents (see the corresponding boldfaced numbers). In the tables, we have also reported which ranges of N have been considered for the best fits to the data. Unfortunately, for θ_{path} and t_{path} an analogous scheme cannot be applied because we have data only for very limited ranges of l. Then, our best estimates come from simply averaging single values together (see boldfaced numbers in Table III).

2. Extrapolating scaling exponents of tree contacts

Tabulated values for intrachain contacts, $\langle N_c(N) \rangle \sim N^{\gamma_c}$, and interchain contacts in tree melts, $\langle N_c^{\text{inter}}(N) \rangle \sim N^{\beta}$, are given in Table V. Corresponding extrapolated values of critical

exponents γ_c and β were obtained by the same methodology reported in our previous articles [18,19]. For brevity, it was summarized in the caption of Table V. Otherwise, the interested reader can look into the above-mentioned works for more details.

In all cases, the quality of the fits is estimated by standard statistical analysis [39]: normalized χ-square test $\tilde{\chi}^2 \equiv \frac{\chi^2}{D-f}$, where $D - f$ is the difference between the number of data points, D, and the number of fit parameters, f. When $\tilde{\chi}^2 \approx 1$ the fit is deemed to be reliable. The corresponding $\mathcal{Q}(D - f, \chi^2)$ values provide a quantitative indicator for the likelihood that χ^2 should exceed the observed value, if the model were correct [39]. The results of all fits (Tables II–V) are reported together with the corresponding errors, $\tilde{\chi}^2$ and $\mathcal{Q}$ values. Unless otherwise said, all error bars for the estimated asymptotic values (boldfaced numbers in Tables II–V) are written in the form $\pm$(statistical error)$\pm$(systematic error), where the "statistical error" is the largest value obtained from the different fits [13] and the "systematic error" is the spread between the single estimates. For brevity, these are combined together into one single error bar in Table I as $\sqrt{(\text{statistical error})^2 + (\text{systematic error})^2}$.

IV. RESULTS AND DISCUSSION

We begin with distribution functions for observables characterizing the tree connectivity: the distribution of branch

TABLE I. Critical exponents for distribution functions of lattice trees. (Top panel) Theoretical predictions by using the results of the Flory theory for ν_{path}, ρ, and ν [18,19]. (Bottom) Corresponding numerical results obtained by: (a) Extrapolation to $N \to \infty$ of "effective" exponents for trees of size N; see also Tables II–V for details. (b) Substitution of numerical asymptotic exponents (from Refs. [18,19] and this work) into the scaling relations summarized in the top. Mean values and corresponding error bars have been rounded to the first significant decimal digit.

	Flory theoretical values of critical exponents					
	Relation to other exponents	Ideal trees, annealed connect.	2d melt of trees, annealed connect.	3d melt of trees, annealed connect.	3d self-avoiding trees, annealed connect.	3d self-avoiding trees, quenched ideal connect.
θ_l	$=\frac{1}{\rho} - 1$	1	$\frac{1}{2} = 0.5$	$\frac{4}{5} = 0.8$	$\frac{4}{9} \approx 0.444$	–
t_l	$=\frac{1}{1-\rho}$	2	3	$\frac{9}{4} = 2.25$	$\frac{13}{4} = 3.25$	–
θ_{path}	–	0	>0	>0	>0	>0
t_{path}	$=\frac{1}{1-\nu_{\text{path}}}$	2	4	$\frac{5}{2} = 2.5$	$\frac{9}{2} = 4.5$	∞
θ_{tree}	$\min(\theta_{\text{path}}, \frac{1}{\nu} - d)$	0	0	0	$-\frac{8}{7} \approx -1.143$	-1
t_{tree}	$=\frac{1}{1-\nu}$	$\frac{4}{3} \approx 1.333$	2	$\frac{3}{2} = 1.5$	$\frac{13}{6} \approx 2.167$	2
γ_c	$=2 - \nu(d + \theta_{\text{tree}})$	$\frac{5}{4} = 1.25$	1	1	1	1
β	$=2 - \nu(d + \theta_{\text{path}})$	–	$1 - \frac{\theta_{\text{path}}}{2} < 1$	$1 - \frac{\theta_{\text{path}}}{3} < 1$	–	–

|	Numerical values of critical exponents									
	Ideal trees, annealed connect.		2d melt of trees, annealed connect.		3d melt of trees, annealed connect.		3d self-avoiding trees, annealed connect.		3d self-avoiding trees, quenched ideal connect.	
	(a)	(b)	(a)	(b)	(a)	(b)	(a)	(b)	(a)	(b)
θ_l	1.1 ± 0.2	1.0 ± 0.2	0.593 ± 0.003	0.63 ± 0.02	0.85 ± 0.07	0.9 ± 0.2	0.53 ± 0.02	0.56 ± 0.05	–	–
t_l	2.0 ± 0.1	2.0 ± 0.2	2.35 ± 0.01	2.58 ± 0.05	2.17 ± 0.07	2.1 ± 0.2	2.435 ± 0.006	2.8 ± 0.2	–	–
θ_{path}	0	–	0.63 ± 0.04	–	0.28 ± 0.02	–	1.07 ± 0.08	–	1.23 ± 0.07	–
t_{path}	2	2.04 ± 0.04	4.2 ± 0.1	4.6 ± 0.1	2.7 ± 0.1	2.46 ± 0.04	3.8 ± 0.1	3.9 ± 0.3	3.8 ± 0.2	7.7 ± 1.8
θ_{tree}	-0.1 ± 0.2	0	-0.14 ± 0.02	0.08 ± 0.09	-0.3 ± 0.1	0.1 ± 0.2	-0.96 ± 0.02	-0.9 ± 0.2	-0.84 ± 0.07	-0.8 ± 0.3
t_{tree}	1.3 ± 0.3	1.33 ± 0.04	1.857 ± 0.005	1.92 ± 0.07	1.52 ± 0.04	1.47 ± 0.04	2.19 ± 0.02	1.9 ± 0.2	2.10 ± 0.01	1.9 ± 0.2
γ_c	1.27 ± 0.02	1.3 ± 0.1	1.00 ± 0.08	1.11 ± 0.05	1.1 ± 0.1	1.14 ± 0.09	0.98 ± 0.02	1.02 ± 0.09	1.00 ± 0.02	1.0 ± 0.2
β	–	–	0.628 ± 0.002	0.74 ± 0.07	0.881 ± 0.003	0.95 ± 0.07	–	–	–	–
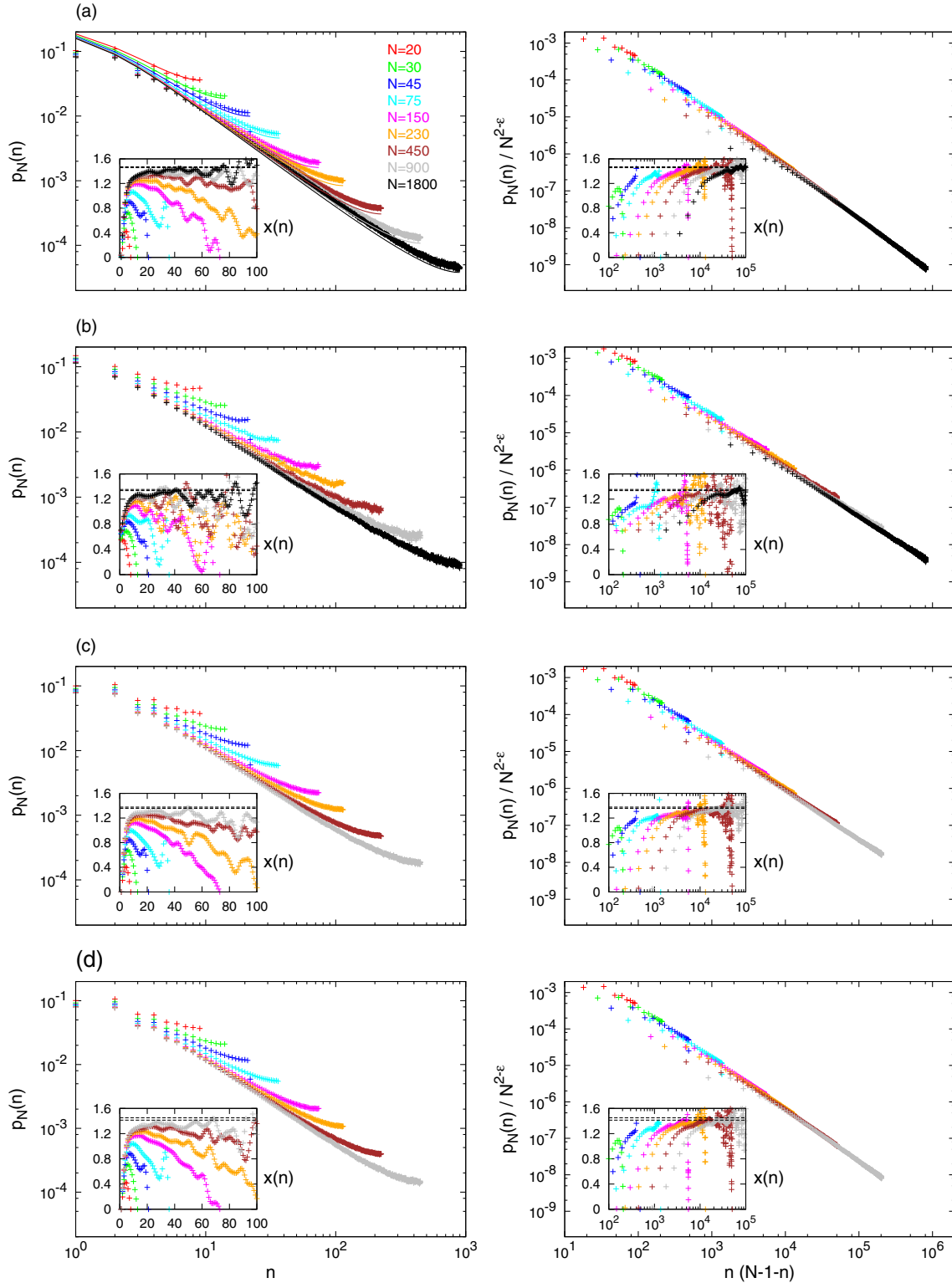
FIG. 1. Distribution functions of branch weight n, $p_N(n)$, for trees of total mass N (left-hand side panels) and the same distributions rescaled by $N^{2-\epsilon}$ and as functions of $n(N-1-n)$ (right-hand side panels). Data for (a) ideal trees, with solid lines in the left-hand side panel corresponding to Eq. (9); (b) $3d$ self-avoiding trees with annealed connectivity; (c, d) $2d$ and $3d$ melt of trees. Left-hand side and right-hand side insets show the differential fractal exponents $x = x(n) \equiv -\frac{\log p_N(n+1)/p_N(n)}{\log(n+1)/n}$ and $x = x(n) \equiv -\frac{\log p_N[(n+1)(N-2-n)]/p_N[n(N-1-n)]}{\log[(n+1)(N-2-n)]/[n(N-1-n)]}$ (data were smoothed for better visualization) compared to the asymptotic scaling relation $\lim_{n\to\infty} x(n) = 2 - \epsilon$ (the narrow strip within dashed lines, corresponding to the best estimates "$\epsilon \pm$ (error bars)" as reported in Refs. [18,19]).
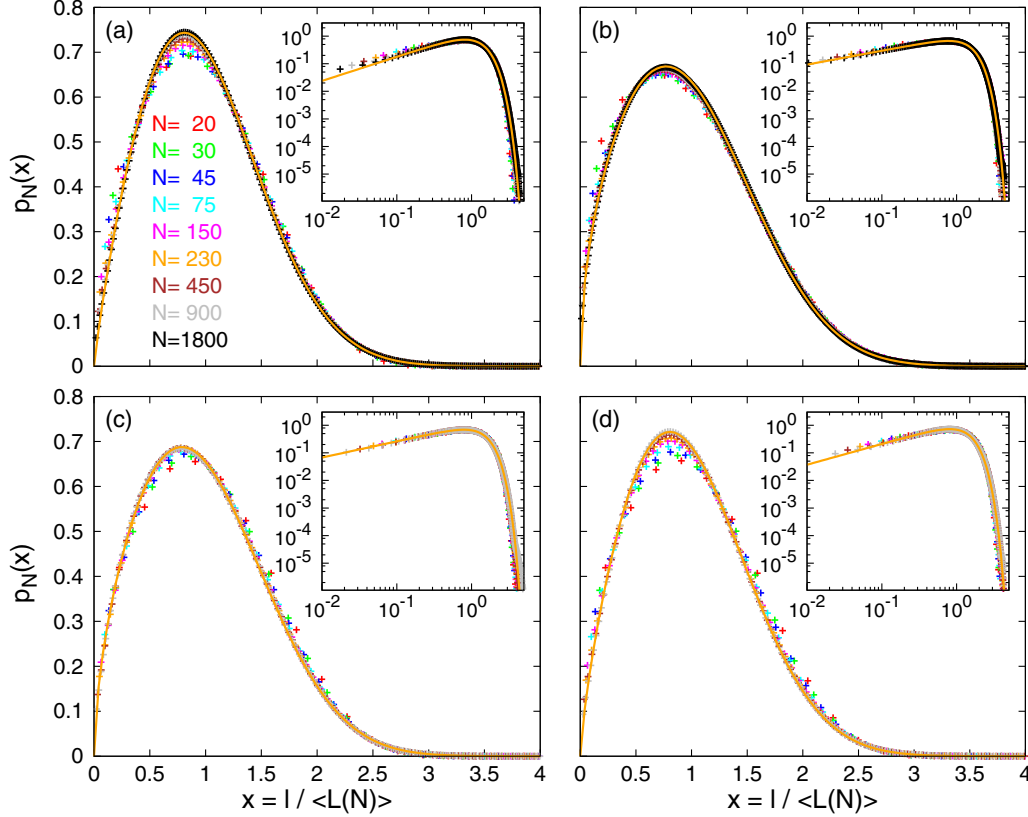
FIG. 2. Distribution functions, $p_N(l)$, of linear paths of length l for trees of total mass N. Data for: (a) ideal trees; (b) $3d$ self-avoiding trees with annealed connectivity; (c, d) $2d$ and $3d$ melt of trees. Orange solid lines correspond to the one-dimensional Redner-des Cloizeaux function, Eq. (26), with parameters θ_l and t_l obtained from the best fits to data for $N = 1800$ (ideal and self-avoiding trees) and $N = 900$ ($2d$ and $3d$ melt of trees); see Table II for detailed values of fit parameters. Inset: same plots in log-log representation.

weights (Sec. IV A) and path lengths (Sec. IV B). Then, we turn to the conformational statistics of linear path on the tree (Sec. IV C) and the distribution of internal distances (Sec. IV D).

A. Branch weight statistics and generalized Kramers relation

In Fig. 1 we show the distribution, $p_N(n)$, of the weight, n, of the branches generated by cutting randomly selected bonds in trees of size N. Obviously, it is possible to cut larger branches from larger trees, but independently of N the vast majority of the branches is small. This follows immediately from the fact that for all our systems a large fraction ($\approx 40\%$ for ideal and melt of trees and $\approx 27\%$ for annealed self-avoiding trees [18,19]) of the nodes is one-functional: cutting the bonds joining them to the tree generates branches of weight $n = 0$.

To gain some intuition for the form of these distributions, it is useful to reconsider the case of ideal trees [Sec. I, Eqs. (7)–(9)], where $\mathcal{Z}_n \sim e^{2\lambda n}/(\lambda n)^{3/2}$. In that case, $p_N(n) \sim \frac{N^{3/2}}{n^{3/2}(N-n-1)^{3/2}}$, which simplifies to $p_N(n) \sim n^{-3/2}$ for small $1 < n \ll N$. As expected, by plotting data for $p_N(n)$ in log-log plots as a function of n (left-hand column of Fig. 1) we find good agreement with the expected power law for small n, while plotting data as a function of $n(N - 1 - n)$ (right-hand side) produces nearly perfect power-law behavior over the entire range $1 \leqslant n \leqslant N/2$.

Interestingly, we find similar power-law behavior for interacting trees, too. We therefore tentatively generalize Eq. (7) for the tree partition function to

$$\mathcal{Z}_n \sim c^n n^{-x}. \tag{24}$$

In fact, this form is compatible with the Kramers theorem, Eq. (8), since $\sum_{n=0}^{N-1} \mathcal{Z}_n \mathcal{Z}_{N-1-n} = c^N \sum_{n=0}^{N-1} n^{-x}(N - 1 - n)^{-x} \sim c^N N^{-x} = \mathcal{Z}_N$. The resulting average branch weight of $\langle N_{br}(N) \rangle \sim N^{2-x}$ implies $x = 2 - \epsilon$. As shown in the corresponding insets, the relation $x = 2 - \epsilon$ is well satisfied with values for ϵ taken from Refs. [18,19]. The numerical prefactor c is related to the asymptotic branching probability (see Fig. 4 in Ref. [18] and Fig. 3 in Ref. [19]), since in the limit $N \to \infty$, $\langle n_3 \rangle/N = \langle n_1 \rangle/N = 2 p_N(n = 0)$ [18], and $p_N(n = 0) = \mathcal{Z}_{N-1}/\mathcal{Z}_N = c^{-1}(\frac{N-1}{N})^{\epsilon-2} \simeq c^{-1}$.

B. Path length statistics for trees

As illustrated in Fig. 2, the measured path length distribution functions, $p_N(l)$, fall onto universal master curves, when plotted as a function of the rescaled path length $x = l/\langle L(N) \rangle$:

$$p_N(l) = \frac{1}{\langle L(N) \rangle} q \left(\frac{l}{\langle L(N) \rangle} \right). \tag{25}$$

These master curves are well described by the one-dimensional Redner-des Cloizeaux (RdC) form (orange lines in Fig. 2):

$$q(x) = C_l \, x^{\theta_l} \, \exp[-(K_l x)^{t_l}]. \tag{26}$$

The constants,

$$C_l = t_l \, \frac{\Gamma^{\theta_l+1}[(\theta_l+2)/t_l]}{\Gamma^{\theta_l+2}[(\theta_l+1)/t_l]}, \tag{27}$$

$$K_l = \frac{\Gamma[(\theta_l+2)/t_l]}{\Gamma[(\theta_l+1)/t_l]}, \tag{28}$$

follow from the conditions that $p_N(l)$ is normalized to 1 and that the *first* moment, $\langle L(N) \rangle$, is the only relevant scaling variable. Estimated values for (θ_l, t_l) obtained from best fits

of Eq. (26) to data for specific values of N and extrapolated values to large N are summarized in Table II.

Interestingly, we can give a physical interpretation of the observed (effective) exponents. For small path lengths, results are not affected by the total tree size. We thus expect to find $n(l_{\max}) \sim l_{\max}^{1/\rho}$ segments at a contour distance $l \leqslant l_{\max}$ from any node. Since $p(l_{\max}) \sim dn(l_{\max})/dl_{\max}$, this suggests the scaling relationship

$$\theta_l = \frac{1}{\rho} - 1. \tag{29}$$

To estimate the probability for observing very long paths, it is tempting to adjust the Pincus-blob argument [35] cited in
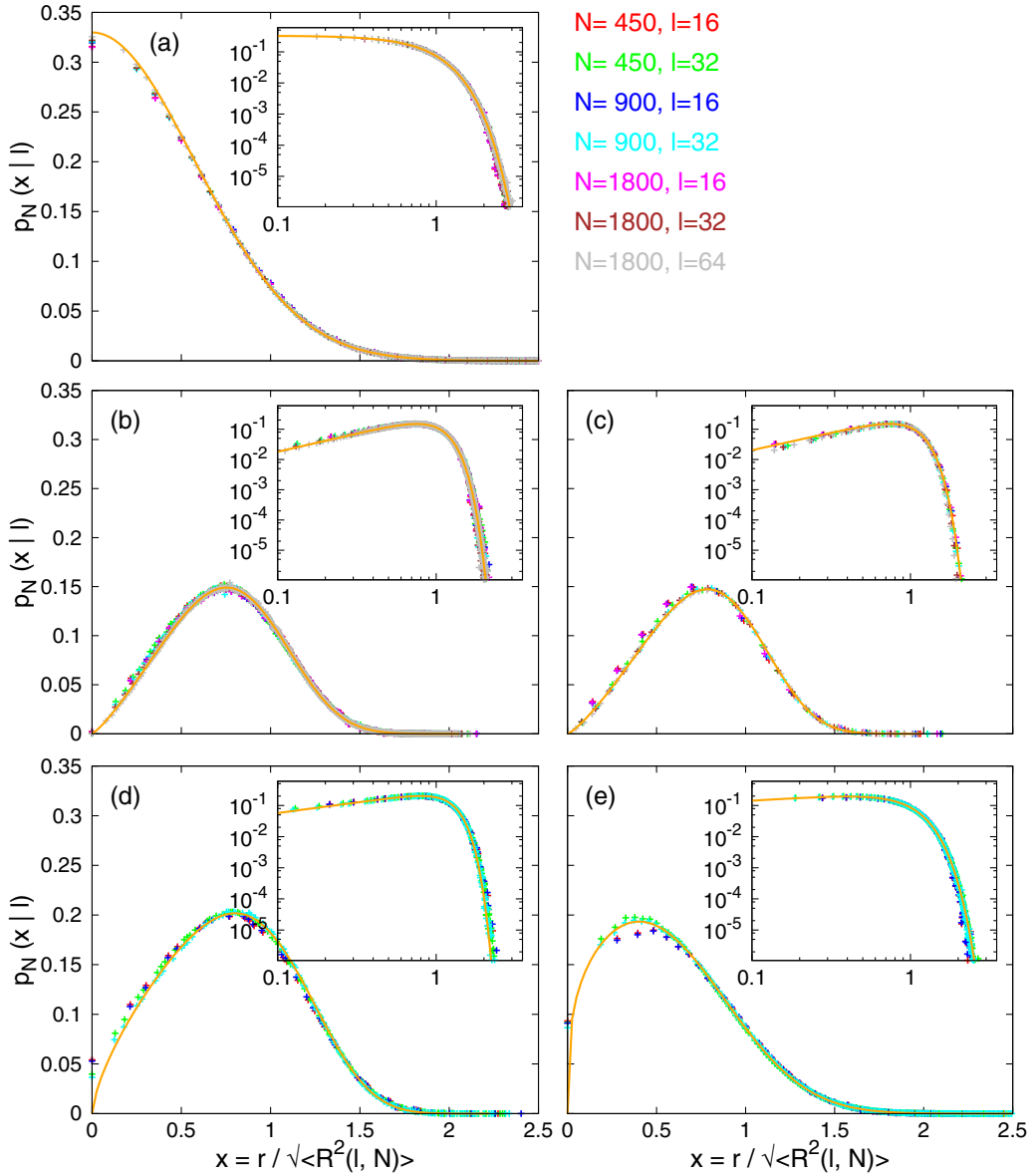
FIG. 3. Distribution functions, $p_N(r|l)$, of end-to-end spatial distances, r, for linear paths of length l on trees of total mass N. Data for: (a) ideal trees; (b, c) $3d$ self-avoiding trees with annealed and quenched ideal connectivities; (d, e) $2d$ and $3d$ melt of trees. Orange solid lines correspond to theoretical predictions: for ideal trees data match the Gaussian distribution, while melt of trees and self-avoiding trees are described by the Redner-des Cloizeaux function, Eq. (32), with parameters θ_{path} and t_{path} obtained from the best fits to data for $N = 1800$ and $l = 64$ (self-avoiding trees) and $N = 900$ and $l = 32$ (melt of trees); see Table III for detailed values of fit parameters. Insets: Same plots in log-log representation.

Sec. II C. A stretched tree should behave like a string of N/g unperturbed trees of size $\xi \sim g^{\rho}$, suggesting that

$$t_l = \frac{1}{1 - \rho}. \qquad (30)$$

The argument works well [see bottom panel of Table I, columns (a) and (b)] when comparing the asymptotic values for t_l in different ensembles to the corresponding numerical values for ρ taken from Refs. [18,19]. Interestingly, being only functions of ρ, θ_l, and t_l can also be explicitly calculated in terms of results for ρ from the Flory theory [18,19]; see top panel of Table I. Interestingly, the Flory theory gives a remarkable accurate prediction for most of the cases discussed.

C. Conformational statistics of linear paths

Figure 3 shows measured end-to-end vector distributions, $p_N(\vec{r}|l)$, for paths of length l on trees of mass N. The data superimpose, when expressed as functions of the scaled distances, $x = |\vec{r}|/\sqrt{\langle R^2(l,N) \rangle}$:

$$p_N(\vec{r}|l) = \frac{1}{\langle R^2(l,N) \rangle^{3/2}} \, q\left(\frac{|\vec{r}|}{\sqrt{\langle R^2(l,N) \rangle}} \right). \qquad (31)$$

Moreover, they are in excellent agreement with the RdC distribution [Eqs. (18), (20), and (21) and orange lines in Fig. 3]:

$$q(x) = C \, x^{\theta_{\text{path}}} \, \exp(-(Kx)^{t_{\text{path}}}). \qquad (32)$$

The shape of the rescaled distributions, and hence the characteristic exponents, θ_{path} and t_{path}, depend on the universality class. Not surprisingly, paths on ideal trees are well described by the Gaussian distribution; i.e., $\theta_{\text{path}} = 0$ and $t_{\text{path}} = 2$. Fitted values for the other cases are listed in Table III. Given the limited range of available path lengths l, we have found no meaningful way to estimate asymptotic values. We have then simply taken the average of the available fitted values (see boldfaced numbers in Table III). Again, the observed values can be given a physical interpretation.

The exponent θ_{path} describes the reduction of the contact probability, Eq. (15), relative to a naïve Gaussian estimate. Importantly, it is a genuinely novel exponent, i.e., it is *independent* from all other exponents discussed in Refs. [18,19] and in this work. In the case of self-avoiding walks, θ is related to the entropy exponent γ, Eq. (16) [27,30]. Interestingly, Grosberg and colleagues argued [24] that the identical Flory predictions of $\nu = 3/(d+2)$ for self-avoiding walks and for the path statistics in melts of annealed lattice trees suggests a deeper analogy between the two problems [8]. Using $\gamma_{2d} \approx 1.344$ and $\gamma_{3d} \approx 1.162$ for two- and three-dimensional self-avoiding walks [30] and Eq. (16) suggests $\theta_{\text{path},2d} \approx 0.459$ and $\theta_{\text{path},3d} \approx 0.276$. In particular, the $3d$ value is in very good agreement with our finding $\theta_{3d} = 0.28 \pm 0.02$ (Tables I and III), while the $2d$ value appears smaller than the reported $\theta_{2d} = 0.63 \pm 0.04$. Notice though, that these exponents were measured for path length $l = \mathcal{O}(50)$ and then finite-size effects may likely induce a bias on the final result.

The exponent t_{path} controls the nonlinear path elasticity at large elongations. The measured effective values can be compared to the Fisher-Pincus relation, Eq. (19), for self-

avoiding walks [34,35],

$$t_{\text{path}} = \frac{1}{1 - \nu_{\text{path}}}, \qquad (33)$$

where specific values for ν_{path} are taken from Refs. [18,19]; see bottom panel of Table I, columns (a) and (b). In general, agreement is overall good. The only exception is for $3d$ self-avoiding trees with quenched ideal statistics, which, again, may be ascribed to the limited range of path lengths of our simulated trees. As for θ_l and t_l and being a function of ν_{path} only, specific values for t_{path} can be also obtained by using the Flory results [18,19] for ν_{path} (top panel of Table I): again, for most of the cases, there exist fair agreement with numerical predictions.

D. Conformational statistics of trees

Figure 4 (left panels) shows distributions $p_N(\vec{r})$ of vectors $\vec{r}$ connecting all tree nodes. The data superimpose, when expressed as functions of the scaled distances, $x = |\vec{r}|/\sqrt{2 \langle R_g^2(N) \rangle}$:

$$p_N(\vec{r}) = \frac{1}{\left(2 \langle R_g^2(N) \rangle \right)^{3/2}} \, q\left(\frac{|\vec{r}|}{\sqrt{2 \langle R_g^2(N) \rangle}} \right). \qquad (34)$$

Again, the distributions are in excellent agreement with the RdC form [Eqs. (18), (20), and (21) and orange lines in Fig. 4]:

$$q(x) = C \, x^{\theta_{\text{tree}}} \, \exp\left(-(Kx)^{t_{\text{tree}}} \right). \qquad (35)$$

The extracted exponents and corresponding extrapolations to $N \to \infty$ are listed in Table IV.

In the following, we relate the characteristic exponents θ_{tree} and t_{tree} to our previous results by using Eqs. (32) and (26) together with the convolution identity,

$$p_N(r) = \int_0^{\infty} p_N(r|l) \, p_N(l) \, dl, \qquad (36)$$

which states that the local density can be calculated by adding up the contributions from paths of all possible length, $1 \leqslant l \leqslant N$. The behavior of $p_N(r)$ for large distances, $r > R_g$, can be estimated from the contour distance $l^*(r)$, which makes the dominant contribution to particle pairs found at the spatial distance r. Combining the arguments of the compressed exponentials in Eqs. (26) and (32), this requires the minimization of $(\frac{l}{\langle L(N) \rangle})^{t_l} + (\frac{r}{\sqrt{\langle R^2(l) \rangle}})^{t_{\text{path}}}$ and yields

$$t_{\text{tree}} = \frac{t_l \, t_{\text{path}}}{t_l + t_{\text{path}} \, \nu_{\text{path}}} = \frac{1}{1 - \nu}. \qquad (37)$$

Results from computer simulations for asymptotic exponents t_{tree} and ν [18,19] support well this relation [see bottom panel of Table I, columns (a) and (b)].

In the limit of small distances, $r < R_g$, there are two possibilities. If there is no power-law divergence in the small l limit, the integral is dominated by contributions from long paths with $\langle R^2(l) \rangle \gg r^2$, allowing us to set the exponential term in Eq. (32) equal to one. The only r-dependence comes

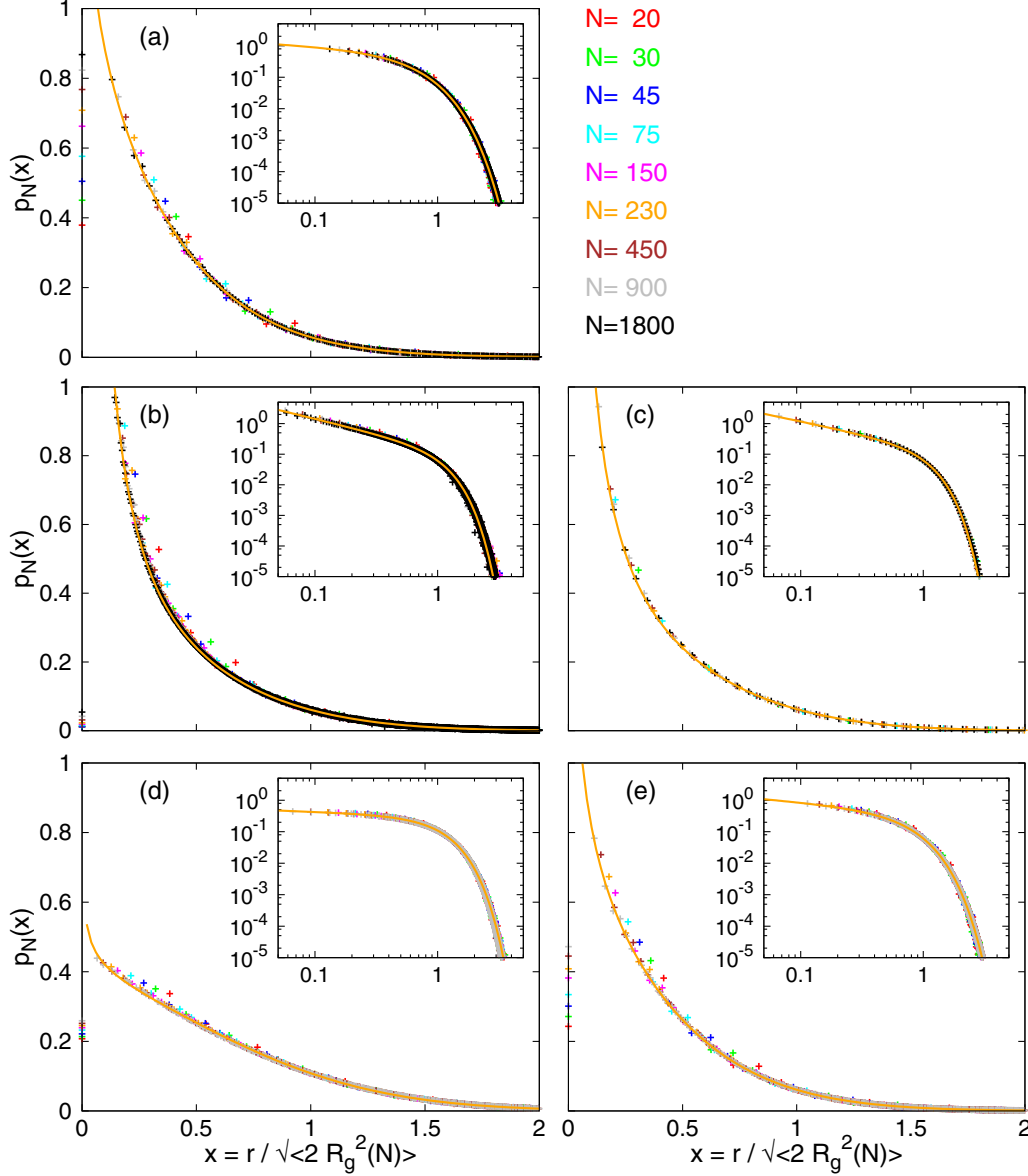FIG. 4. Distribution functions, $p_N(r)$, of spatial distances, r, between pairs of nodes. Data for: (a) ideal trees; (b, c) $3d$ self-avoiding trees with annealed and quenched ideal connectivities; (d, e) $2d$ and $3d$ melt of trees. Orange solid lines correspond to the Redner-des Cloizeaux distribution function, Eq. (35), with parameters θ_{tree} and t_{tree} obtained from the best fits to data with $N = 1800$ (ideal and self-avoiding trees) and $N = 900$ ($2d$ and $3d$ melt of trees); see Table IV for detailed values of fit parameters. Insets: same plots in log-log representation.

through the explicit $r^{\theta_{\text{path}}}$ term and hence,

$$\theta_{\text{tree}} = \theta_{\text{path}} \quad \text{if } \theta_{\text{path}} < \frac{1}{\nu} - d. \tag{38}$$

In the opposite limit, short paths dominate. The apparent divergence of the integrand in the limit $l \to 0$ is removed by the exponential tail of Eq. (32): paths with vanishing contour lengths up to $l \sim r^{1/\nu_{\text{path}}}$ do not contribute to the monomer density for finite spatial distances r. For longer paths, we can set the exponential to one. In this case,

$$\theta_{\text{tree}} = \frac{1}{\nu} - d \quad \text{if } \frac{1}{\nu} - d < \theta_{\text{path}}. \tag{39}$$

Summarizing,

$$\theta_{\text{tree}} = \min\left(\theta_{\text{path}}, \frac{1}{\nu} - d\right) \tag{40}$$

$$= \begin{cases} 0 & \text{for ideal trees in } d \leqslant 4 \\ \frac{1}{\nu} - d & \text{else} \end{cases}, \tag{41}$$

since $\theta_{\text{path}} \equiv 0$ for ideal trees and since we expect $\theta_{\text{path}} > 0$ and $\nu \geqslant 1/d$ for interacting trees. Table I compares the asymptotic results to theoretical predictions. Again, the general agreement is fairly good. Finally, as for θ_l, t_l, and t_{path}, specific values for θ_{tree} and t_{tree} can be calculated by resorting to the Flory results for ν (top panel of Table I). Once again, the predictions prove to be remarkably accurate.
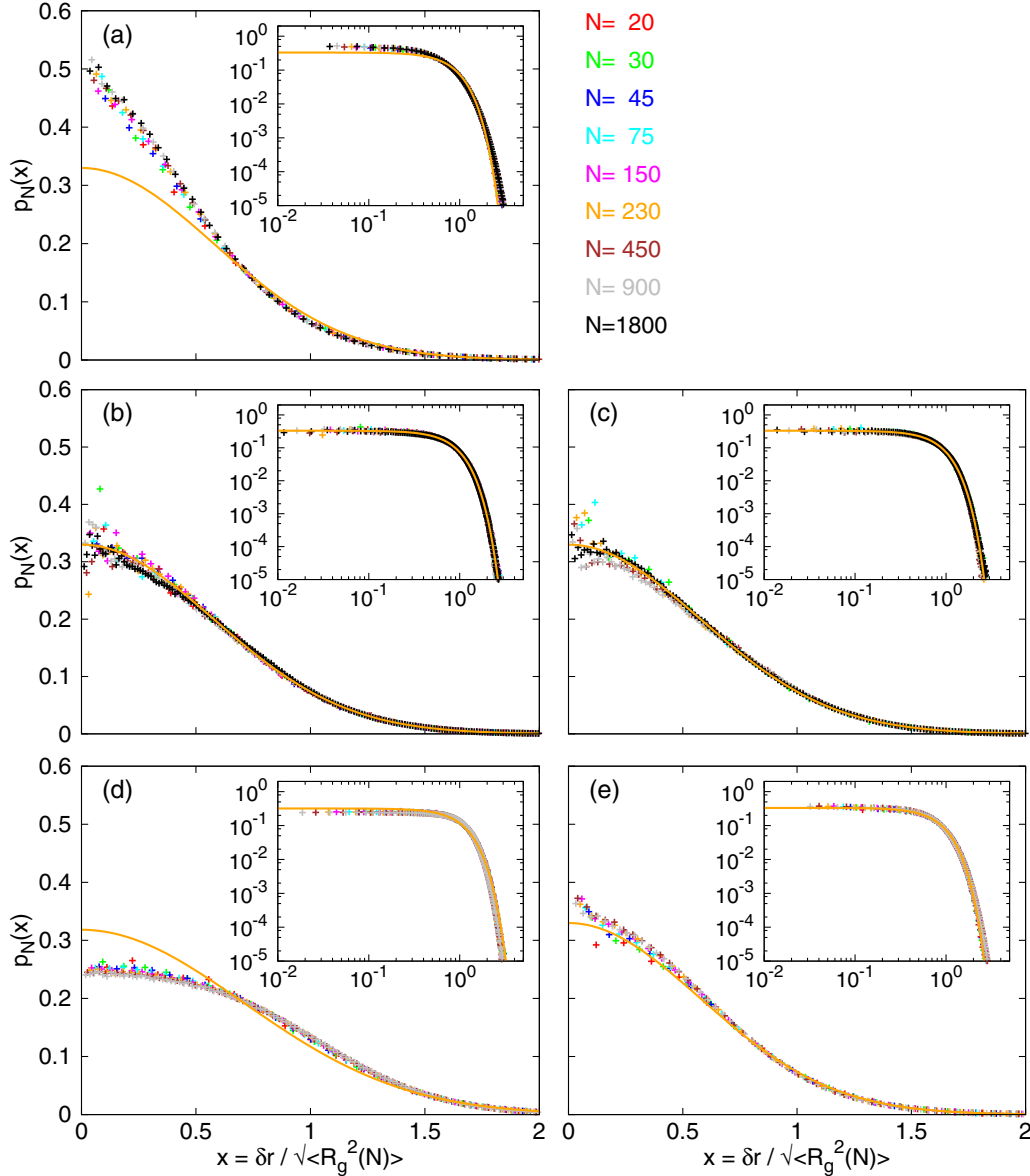
FIG. 5. Distribution functions of spatial distances, $\vec{\delta r}$, of nodes from the tree center of mass, compared to the Gaussian distribution (yellow line). Data for: (a) ideal trees; (b, c) $3d$ self-avoiding trees with annealed and quenched ideal connectivities; (d, e) $2d$ and $3d$ melt of trees. Insets: same plots in log-log representation.

To conclude the section, in Fig. 5 we focus on the distribution functions, $p_N(\vec{\delta r})$, of nodes spatial distances from the centers of mass of corresponding trees. Clearly, for the central node this distribution is Gaussian. On the other hand, distant nodes cannot distinguish between the central node and the tree center of mass and their positions hence follow again a RdC distribution. Averaged over node identities, the monomer distribution around the tree center of mass seems to become Gaussian for self-avoiding trees [Figs. 5(b) and 5(c)], but *not* for ideal trees or trees in melt [Figs. 5(a), 5(d), and 5(e)]. Interestingly, the latter effect was already noted a long time ago for *ideal* linear chains [40].

E. Self-contacts

We turn then to the average number of self-contacts per tree, $\langle N_c(N) \rangle \sim N^{\gamma_c}$ (left-hand panel of Fig. 6 and Table V).

Consider an arbitrary pair of monomers. The probability to find them in close contact scales as $N^{-\nu(d+\theta_{\text{tree}})}$. Since there are $\mathcal{O}(N^2)$ different monomer pairs, we have

$$\gamma_c = 2 - \nu(d + \theta_{\text{tree}}) \tag{42}$$
$$= \begin{cases} 2 - \frac{d}{4} & \text{for ideal trees in } d \leqslant 4 \\ 1 & \text{else} \end{cases} .$$

This prediction compares extremely well with our numerical estimates for γ_c; see Table I. Note that the mean-field estimate $\gamma_c = 2 - d\nu$ holds only for ideal trees in $d \leqslant 4$ dimensions. The melt case is marginal in that we expect $\nu = 1/d$ and thus $\gamma_c = 1$: by using the estimated asymptotic values of ν in $2d$ and $3d$ [19] and θ_{tree}, the different values for γ_c compare well for all studied ensembles [see bottom panel of Table I, columns (a) and (b)]. In all other cases, $\gamma_c = 1$ independently of ν, θ_{path} and θ_{tree}, indicating that the local monomer density is finite
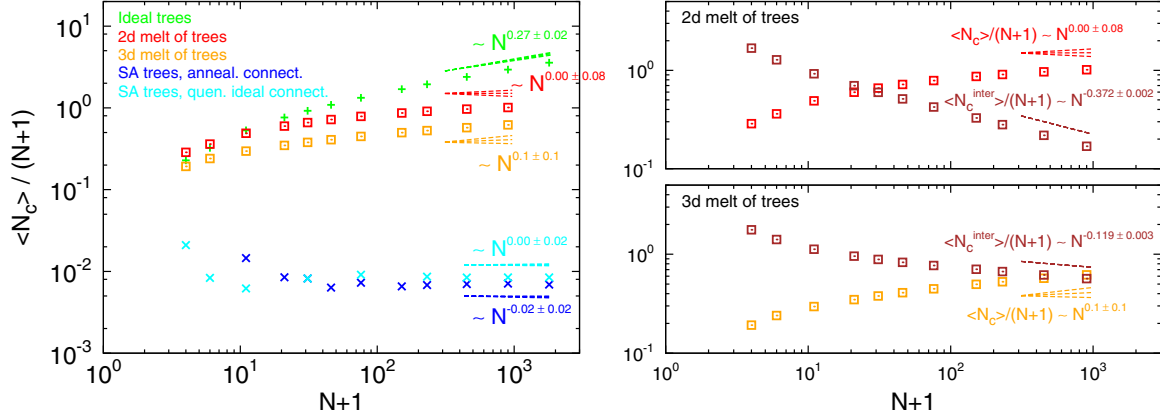
FIG. 6. (Left) Average number of *intra*-chain contacts per node, $\langle N_c(N)\rangle/(N+1) \sim N^{\gamma_c-1}$, in the different ensembles. (Right) Comparison to the average number of *inter*-chain contacts per node, $\langle N_c^{\mathrm{inter}}\rangle/(N+1) \sim N^{\beta-1}$, in 2d and 3d melts. Dashed lines mark the ranges of corresponding asymptotic behaviors with scaling exponents γ_c and β; see Table I.

and independent of tree size. This is yet another illustration of the subtle cancellation of errors in Flory arguments, which are built on the mean-field estimates of contact probabilities [26].

For tree melts, we have also considered the average number of contacts between nodes on *different* trees, $\langle N_c^{\mathrm{inter}}(N)\rangle \sim N^{\beta}$ (right-hand panels of Fig. 6 and Table V). In the melt, the average number of contacts per node $\frac{\langle N_c(N)\rangle}{N} + \frac{\langle N_c^{\mathrm{inter}}(N)\rangle}{N}$ is N-independent (see also Table V), hence $\beta \approx 1 - \Delta$, where Δ is the exponent of the power-law correction to the large-N behavior of $\langle N_c(N)\rangle$: $\langle N_c(N)\rangle \approx a\,N^{\gamma_c}(1 - b\,N^{-\Delta}) = a\,N(1 - b\,N^{-\Delta})$ with a and b numerical prefactors. Δ can be calculated by considering the two leading terms in Eq. (36) for small r's after substituting the upper bound of the integral with $\mathcal{O}(N^{\rho})$. Since $\theta_{\mathrm{path}} > \frac{1}{\nu} - d$ we get $p_N(r) \sim (\frac{r}{N^{\nu}})^{1/\nu-d}(1 - \mathcal{O}(\frac{r}{N^{\nu}})^{d+\theta_{\mathrm{path}}-1/\nu})$. The average number of self-contacts per tree $\langle N_c(N)\rangle$ is proportional to the integral of the former expression from 0 to some small cutoff spatial distance, or $\langle N_c(N)\rangle = a\,N(1 - b\,N^{1-\nu(d+\theta_{\mathrm{path}})})$. Consequently, $\Delta = -1 + \nu(d + \theta_{\mathrm{path}})$ and

$$\beta = 1 - \Delta = 2 - \nu(d + \theta_{\mathrm{path}}). \tag{43}$$

In particular, Eq. (43) implies that $\beta < 1$. By employing the asymptotic values of ν [19] and θ_{path}, Eq. (43) shows good agreement with direct estimates of β values [see bottom panel of Table I, columns (a) and (b)].

V. SUMMARY AND CONCLUSION

In the present article, we have pursued our investigation of the conformational statistics of various types of lattice trees with volume interactions [18,19,25]: 2d and 3d melts of lattice trees with annealed connectivity as well as 3d self-avoiding lattice trees with annealed and with quenched ideal connectivity. The well understood case of ideal, noninteracting lattice trees with annealed connectivity [14,15] always serves as a useful reference. Here we have complemented the earlier analyses [18,19] of the average behavior by reporting results for distribution functions for observables characterizing tree conformations and connectivities. In particular, we found that branch weight distributions follow a generalized Kramers relation, Eq. (8), with $\mathcal{Z}_n \sim c^n n^{\epsilon-2}$ and

that path length and distance distributions are non-Gaussian and closely follow Redner-des Cloizeaux [27,33] distributions Eqs. (25), (26); (31), (32); and (34), (35) of the type

$$p_N(\vec{r}) = \left(\frac{1}{\langle r^2\rangle_N}\right)^{d/2} q\left(\frac{|\vec{r}|}{\sqrt{\langle r^2\rangle_N}}\right),$$

$$q(\vec{x}) = C(\theta,t)\,|x|^{\theta}\,\exp(-(K(\theta,t)\,|x|)^t),$$

which are fully characterized by pairs of additional exponents, θ and t, summarized in Table I. The various exponents t describe the compressed exponential large distance (large path length) behavior of the distribution. Our results suggest that they obey generalized Fisher-Pincus [34,35] relations, Eqs. (30), (33), and (37). The exponents θ characterize small distance (small path length) power-law behavior and are hence related to contact probabilities [Eqs. (42) and (43)]. We have related them to each other and the other tree exponents [Eqs. (29) and (40)]. The only exception is the exponent θ_{path} for the small distance behavior of the path end-to-end distance distribution. The situation is similar to the well-known case of linear self-avoiding walks, where the corresponding exponent θ and the closure probability are related to the entropy exponent γ, which cannot be predicted by Flory theory. Additional work is required to corroborate the proposed relation [8] between the self-avoiding walk exponents and those characterising tree melts.

In conclusion, interacting randomly branching polymers exhibit an extremely rich behavior and swell by a combination of modified branching and path stretching [24]. As previously shown [25], the average behavior [18,19] in the various regimes and crossovers can be well described by a generalized Flory theory. Our present results demonstrate that this is not the case for distribution functions. Nonetheless, their non-Gaussian functional form can be characterized by a small set of exponents, which are related to each other and the standard trees exponents. The good agreement of the predicted relations with the numerical data suggests that we now dispose of a coherent framework for describing the connectivity and conformational statistics of interacting trees in a wide range of situations.

APPENDIX: SUPPLEMENTAL TABLES

The Appendix contains four supplemental tables reporting the measured values for the effective and asymptotic exponents introduced and discussed in this work. Specifically: (1) Table II is for exponents θ_l and t_l (path length statistics, discussed in Sec. IV B); (2) Table III is for exponents θ_{path} and t_{path} (conformational statistics of linear paths, discussed in Sec. IV C); (3) Table IV is for exponents θ_{tree} and t_{tree} (conformational statistics of trees, discussed in Sec. IV D); (4) Table V is for exponents γ_c and β (intrachain and interchain contacts, discussed in Sec. IV E).

TABLE II. Path length statistics. Effective exponents θ_l and t_l obtained by best fits of the Redner-des Cloizeaux function, Eq. (26), to the numerical distributions $p_N(l)$ of linear paths of length l at different N (Fig. 2). Extrapolations to $N \to \infty$ were obtained by employing three-(Δ as free parameter) and two-parameter (Δ fixed to 1) fit functions, see Sec. III C. Final estimates with corresponding statistical and systematic errors are given at the end of the table (in boldface).

			θ_l	
N	Ideal trees	$2d$ melt of trees	$3d$ melt of trees	Self-avoid. trees anneal. connect.
20	0.525 ± 0.034	0.390 ± 0.026	0.391 ± 0.025	0.365 ± 0.038
30	0.537 ± 0.019	0.443 ± 0.017	0.447 ± 0.016	0.365 ± 0.019
45	0.563 ± 0.012	0.484 ± 0.011	0.497 ± 0.010	0.391 ± 0.011
75	0.608 ± 0.009	0.525 ± 0.007	0.556 ± 0.007	0.409 ± 0.006
150	0.677 ± 0.007	0.563 ± 0.004	0.623 ± 0.005	0.443 ± 0.003
230	0.722 ± 0.007	0.580 ± 0.003	0.658 ± 0.004	0.466 ± 0.003
450	0.778 ± 0.005	0.587 ± 0.003	0.708 ± 0.003	0.471 ± 0.002
900	0.831 ± 0.004	0.588 ± 0.002	0.751 ± 0.002	0.486 ± 0.002
1800	0.875 ± 0.003			0.501 ± 0.001
Best fit for $N \geqslant$	20	20	20	20
Δ	0.242 ± 0.027	1.110 ± 0.081	0.390 ± 0.025	0.374 ± 0.001
$\tilde{\chi}^2$	0.750	1.164	0.064	3.786
$\mathcal{Q}$	0.610	0.324	0.997	0.001
$N \to \infty$	1.188 ± 0.075	0.594 ± 0.003	0.905 ± 0.031	0.543 ± 0.011
Best fit for $N \geqslant$	450	230	230	450
Δ	1	1	1	1
$\tilde{\chi}^2$	6.212	0.281	6.780	7.274
$\mathcal{Q}$	0.013	0.596	0.009	0.007
$N \to \infty$	0.909 ± 0.004	0.592 ± 0.003	0.785 ± 0.004	0.512 ± 0.001
	1.049	**0.593**	**0.845**	**0.528**
	±0.075	**±0.003**	**±0.031**	**±0.011**
	±0.140	**±0.001**	**±0.060**	**±0.016**
			t_l	
N	Ideal trees	$2d$ melt of trees	$3d$ melt of trees	Self-avoid. trees anneal. connect.
20	2.787 ± 0.131	3.325 ± 0.152	3.373 ± 0.155	2.394 ± 0.135
30	2.742 ± 0.074	3.043 ± 0.084	3.098 ± 0.083	2.524 ± 0.078
45	2.691 ± 0.045	2.842 ± 0.049	2.879 ± 0.046	2.519 ± 0.045
75	2.599 ± 0.030	2.659 ± 0.026	2.699 ± 0.028	2.536 ± 0.024
150	2.457 ± 0.021	2.513 ± 0.014	2.516 ± 0.016	2.464 ± 0.012
230	2.384 ± 0.018	2.454 ± 0.010	2.441 ± 0.013	2.432 ± 0.009
450	2.290 ± 0.012	2.405 ± 0.008	2.359 ± 0.009	2.422 ± 0.006
900	2.212 ± 0.008	2.384 ± 0.006	2.278 ± 0.006	2.429 ± 0.006
1800	2.169 ± 0.005			2.435 ± 0.002
Best fit for $N \geqslant$	20	20	20	20
Δ	0.273 ± 0.092	0.853 ± 0.141	0.458 ± 0.109	1.110 ± 1.208
$\tilde{\chi}^2$	0.823	0.264	0.401	3.316
$\mathcal{Q}$	0.552	0.933	0.848	0.003
$N \to \infty$	1.911 ± 0.075	2.347 ± 0.012	2.105 ± 0.040	2.431 ± 0.003
Best fit for $N \geqslant$	450	230	230	450
Δ	1	1	1	1
$\tilde{\chi}^2$	0.179	0.059	6.789	0.025
$\mathcal{Q}$	0.672	0.809	0.009	0.873
$N \to \infty$	2.130 ± 0.008	2.360 ± 0.008	2.228 ± 0.008	2.439 ± 0.004
	2.021	**2.353**	**2.167**	**2.435**
	±0.075	**±0.012**	**±0.040**	**±0.004**
	±0.110	**±0.007**	**±0.062**	**±0.004**

TABLE III. Conformational statistics of linear paths. Effective exponents θ_{path} and t_{path} obtained by best fits of the Redner-des Cloizeaux function, Eq. (32), to the numerical distributions $p_N(r|l)$ of end-to-end spatial distances of linear paths of length l at given N (Fig. 3). Final estimates with statistical and systematic errors are given at the end of the table (in boldface).

		2d melt of trees		3d melt of trees		3d self-avoiding trees, annealed connect.		3d self-avoiding trees, quenched *ideal* connect.	
N	l	θ_{path}	t_{path}	θ_{path}	t_{path}	θ_{path}	t_{path}	θ_{path}	t_{path}
450	16	0.596 ± 0.012	4.098 ± 0.045	0.273 ± 0.010	2.749 ± 0.017	1.022 ± 0.022	3.833 ± 0.045	1.141 ± 0.020	3.672 ± 0.047
450	32	0.638 ± 0.005	4.179 ± 0.021	0.278 ± 0.004	2.521 ± 0.006	1.077 ± 0.008	3.698 ± 0.017	1.269 ± 0.014	3.835 ± 0.032
900	16	0.610 ± 0.012	4.127 ± 0.048	0.274 ± 0.011	2.775 ± 0.018	0.991 ± 0.013	3.934 ± 0.028	1.182 ± 0.020	3.587 ± 0.044
900	32	0.682 ± 0.006	4.324 ± 0.023	0.297 ± 0.004	2.552 ± 0.006	1.095 ± 0.008	3.743 ± 0.015	1.308 ± 0.007	3.901 ± 0.016
1800	16					0.994 ± 0.015	3.960 ± 0.033	1.165 ± 0.019	3.581 ± 0.043
1800	32					1.130 ± 0.004	3.786 ± 0.008	1.298 ± 0.003	3.902 ± 0.007
1800	64					1.210 ± 0.004	3.705 ± 0.008	1.259 ± 0.008	4.058 ± 0.021
		0.631	**4.182**	**0.281**	**2.649**	**1.074**	**3.809**	**1.232**	**3.791**
		±0.012	**±0.048**	**±0.011**	**±0.018**	**±0.022**	**±0.045**	**±0.020**	**±0.047**
		±0.033	**±0.087**	**±0.010**	**±0.114**	**±0.074**	**±0.098**	**±0.063**	**±0.168**

TABLE IV. Conformational statistics of trees. Effective exponents θ_{tree} and t_{tree} obtained by best fits the Redner-des Cloizeaux distribution function, Eq. (35), to the numerical distributions $p_N(r)$ of spatial distances r between tree nodes at different N (Fig. 4). Extrapolations to $N \to \infty$ were obtained by employing three- (Δ as free parameter) and two-parameter (Δ fixed to 1) fit functions; see Sec. III C. The three-parameter fit fails for θ_{tree} of self-avoiding trees with quenched ideal connectivity. In this case, the reported statistical and systematic errors were based on the ones of ideal trees where: (statistical error for three-parameter fit) $\approx$20(statistical error for two-parameter fit) $\approx$2(systematic error). Final estimates with corresponding statistical and systematic errors are given at the end of the table (in boldface).

	θ_{tree}				
N	Ideal trees	2d melt of trees	3d melt of trees	SA trees ann. connect.	SA trees quen. *ideal* connect.
20	1.075 ± 0.522	0.424 ± 0.142	0.409 ± 0.386	-0.617 ± 0.200	–
30	0.518 ± 0.371	0.027 ± 0.059	-0.333 ± 0.156	-0.964 ± 0.088	-0.824 ± 0.020
45	-0.279 ± 0.166	-0.072 ± 0.035	-0.547 ± 0.082	-1.082 ± 0.042	–
75	-0.456 ± 0.086	-0.119 ± 0.018	-0.582 ± 0.039	-1.062 ± 0.022	-0.881 ± 0.003
150	-0.453 ± 0.041	-0.167 ± 0.004	-0.500 ± 0.017	-1.031 ± 0.010	–
230	-0.420 ± 0.026	-0.157 ± 0.003	-0.449 ± 0.011	-1.012 ± 0.007	-0.869 ± 0.004
450	-0.347 ± 0.013	-0.152 ± 0.002	-0.392 ± 0.005	-1.000 ± 0.003	-0.861 ± 0.002
900	-0.272 ± 0.007	-0.144 ± 0.001	-0.347 ± 0.002	-0.986 ± 0.002	-0.857 ± 0.002
1800	-0.225 ± 0.004			-0.978 ± 0.001	-0.842 ± 0.002
Best fit for $N \geqslant$	150	150	150	150	–
Δ	0.323 ± 0.175	0.609 ± 0.379	0.448 ± 1.52	0.492 ± 2.112	–
$\tilde{\chi}^2$	0.493	1.444	0.037	0.230	–
$\mathcal{Q}$	0.611	0.230	0.847	0.794	–
$N \to \infty$	-0.023 ± 0.158	-0.132 ± 0.016	-0.224 ± 0.094	-0.957 ± 0.017	–
Best fit for $N \geqslant$	450	230	230	450	450
Δ	1	1	1	1	1
$\tilde{\chi}^2$	0.454	2.004	2.425	0.223	16.245
$\mathcal{Q}$	0.501	0.157	0.119	0.637	6×10^{-5}
$N \to \infty$	-0.184 ± 0.007	-0.140 ± 0.002	-0.310 ± 0.005	-0.971 ± 0.002	-0.842 ± 0.003
	-0.104	**-0.136**	**-0.267**	**-0.964**	**-0.842**
	±0.158	**±0.016**	**±0.094**	**±0.017**	**±(0.060)**
	±0.081	**±0.004**	**±0.043**	**±0.007**	**±(0.030)**

TABLE IV. (*Continued.*)

				$t_{\rm tree}$	
N	Ideal trees	$2d$ melt of trees	$3d$ melt of trees	SA trees ann. connect.	SA trees quen. *ideal* connect.
20	0.783 ± 0.080	1.253 ± 0.065	0.993 ± 0.094	1.244 ± 0.095	$-$
30	0.900 ± 0.078	1.506 ± 0.045	1.306 ± 0.073	1.604 ± 0.080	1.816 ± 0.022
45	1.192 ± 0.065	1.617 ± 0.034	1.493 ± 0.056	1.845 ± 0.060	$-$
75	1.335 ± 0.047	1.689 ± 0.023	1.608 ± 0.034	2.012 ± 0.044	2.005 ± 0.005
150	1.401 ± 0.027	1.830 ± 0.006	1.597 ± 0.017	2.029 ± 0.023	$-$
230	1.410 ± 0.019	1.827 ± 0.005	1.574 ± 0.011	2.045 ± 0.018	2.104 ± 0.010
450	1.393 ± 0.010	1.850 ± 0.003	1.553 ± 0.005	2.072 ± 0.011	2.096 ± 0.007
900	1.354 ± 0.005	1.849 ± 0.003	1.543 ± 0.003	2.112 ± 0.007	2.080 ± 0.006
1800	1.332 ± 0.003			2.159 ± 0.004	2.127 ± 0.009
Best fit for $N \geqslant$	230	20	75	20	30
Δ	0.240 ± 4.265	1.401 ± 0.101	0.563 ± 0.432	0.609 ± 0.039	1.224 ± 0.110
$\tilde{\chi}^2$	0.961	3.645	0.302	5.354	7.785
$\mathcal{Q}$	0.327	0.003	0.739	2×10^{-5}	3×10^{-5}
$N \to \infty$	1.198 ± 0.283	1.855 ± 0.003	1.516 ± 0.039	2.197 ± 0.016	2.104 ± 0.005
Best fit for $N \geqslant$	450	230	230	450	450
Δ	1	1	1	1	1
$\tilde{\chi}^2$	0.058	4.336	0.004	4.979	16.411
$\mathcal{Q}$	0.809	0.037	0.948	0.026	5×10^{-5}
$N \to \infty$	1.312 ± 0.005	1.859 ± 0.004	1.532 ± 0.005	2.187 ± 0.007	2.104 ± 0.010
	1.255	**1.857**	**1.524**	**2.192**	**2.104**
	± 0.283	**± 0.004**	**± 0.039**	**± 0.016**	**± 0.010**
	± 0.057	**± 0.002**	**± 0.008**	**± 0.005**	**± 0.000**

TABLE V. (Top half of the table) $\langle N_c \rangle/(N+1)$, average number of intrachain contacts per node. $\langle N_c^{\rm inter} \rangle/(N+1)$, average number of interchain contacts per node in tree melts. (Bottom half of the table) Asymptotic ($N \to \infty$) estimation of corresponding critical exponents, γ_c and β. For ideal trees and melt of trees, the numerical extrapolation scheme follows Ref. [13] and was the same adopted in our former works [18,19]. It combines best fits to the data of: (1) single power-law behavior ($\Delta = 0$: $\log \langle N_c \rangle = c_1 + \gamma_c^{\Delta=0} \log N$, for data corresponding to the 3 largest N of each set) and (2) power-law behavior with a correction-to-scaling term ($\Delta \neq 0$: $\log \langle N_c \rangle = c_2 + c_3 N^{-\Delta} + \gamma_c^{\Delta \neq 0} \log N$, for data with $N \gtrsim 10$). The reported values (last line of the table) are calculated as: $\gamma_c = \frac{\gamma_c^{\Delta=0} + \gamma_c^{\Delta \neq 0}}{2} \pm$ (largest statistical error) $\pm$ (spread between $\gamma_c^{\Delta=0}$ and $\gamma_c^{\Delta \neq 0}$), the last being an estimate for systematic errors due to finite-size effects [13]. Equivalent expressions hold for $\langle N_c^{\rm inter} \rangle$. For self-avoiding trees, finite-size effects appear completely negligible: then, γ_c was obtained by fitting data for $N \geqslant 450$ to just the single power-law function.

	Ideal trees	$2d$ melt of trees		$3d$ melt of trees		Self-avoid. trees, annealed connect.	Self-avoid. trees, quen. *ideal* connect.
N	$\langle N_c \rangle/(N+1)$	$\langle N_c \rangle/(N+1)$	$\langle N_c^{\rm inter} \rangle/(N+1)$	$\langle N_c \rangle/(N+1)$	$\langle N_c^{\rm inter} \rangle/(N+1)$	$\langle N_c \rangle/(N+1)$	$\langle N_c \rangle/(N+1)$
3	0.2284 ± 0.0025	0.2865 ± 0.0030	1.6775 ± 0.0038	0.1923 ± 0.0018	1.7675 ± 0.0026	0.0000 ± 0.0000	0.0210 ± 0.0032
5	0.3241 ± 0.0040	0.3610 ± 0.0027	1.2774 ± 0.0033	0.2400 ± 0.0016	1.4079 ± 0.0022	0.0000 ± 0.0000	0.0083 ± 0.0017
10	0.5306 ± 0.0067	0.4890 ± 0.0022	0.9235 ± 0.0023	0.2958 ± 0.0015	1.1255 ± 0.0018	0.0146 ± 0.0056	0.0062 ± 0.0010
20	0.7626 ± 0.0026	0.5990 ± 0.0017	0.6976 ± 0.0017	0.3475 ± 0.0009	0.9572 ± 0.0011	0.0085 ± 0.0009	
30	0.9201 ± 0.0027	0.6604 ± 0.0014	0.5967 ± 0.0013	0.3785 ± 0.0008	0.8861 ± 0.0008	0.0082 ± 0.0007	0.0082 ± 0.0007
45	1.0893 ± 0.0030	0.7190 ± 0.0007	0.5122 ± 0.0007	0.4088 ± 0.0008	0.8291 ± 0.0008	0.0064 ± 0.0005	
75	1.3286 ± 0.0030	0.7861 ± 0.0005	0.4238 ± 0.0005	0.4471 ± 0.0006	0.7703 ± 0.0006	0.0073 ± 0.0005	0.0091 ± 0.0005
150	1.6951 ± 0.0032	0.8660 ± 0.0004	0.3277 ± 0.0004	0.4971 ± 0.0005	0.7042 ± 0.0005	0.0066 ± 0.0003	
230	1.9390 ± 0.0034	0.9078 ± 0.0004	0.2805 ± 0.0003	0.5272 ± 0.0004	0.6685 ± 0.0004	0.0068 ± 0.0002	0.0086 ± 0.0003
450	2.3936 ± 0.0038	0.9648 ± 0.0003	0.2181 ± 0.0002	0.5726 ± 0.0004	0.6177 ± 0.0004	0.0070 ± 0.0002	0.0084 ± 0.0002
900	2.9351 ± 0.0061	1.0115 ± 0.0004	0.1690 ± 0.0003	0.6197 ± 0.0006	0.5680 ± 0.0006	0.0071 ± 0.0001	0.0084 ± 0.0001
1800	3.5665 ± 0.0100					0.0069 ± 0.0001	0.0085 ± 0.0001
	$\langle N_c \rangle \sim N^{\gamma_c}$	$\langle N_c \rangle \sim N^{\gamma_c}$	$\langle N_c^{\rm inter} \rangle \sim N^{\beta}$	$\langle N_c \rangle \sim N^{\gamma_c}$	$\langle N_c^{\rm inter} \rangle \sim N^{\beta}$	$\langle N_c \rangle \sim N^{\gamma_c}$	$\langle N_c \rangle \sim N^{\gamma_c}$
Δ	0.446 ± 0.094	0.214 ± 0.057	1.238 ± 0.217	0.156 ± 0.192	1.129 ± 0.216	$-$	$-$
$\tilde{\chi}^2$	0.803	1.104	0.969	0.739	1.467	$-$	$-$
$\mathcal{Q}$	0.567	0.356	0.435	0.566	0.209	$-$	$-$
	$\gamma_c = 1.253 \pm 0.010$	$\gamma_c = 0.931 \pm 0.018$	$\beta = 0.629 \pm 0.001$	$\gamma_c = 1.011 \pm 0.082$	$\beta = 0.884 \pm 0.001$	$-$	$-$
Δ	0	0	0	0	0	0	0
$\tilde{\chi}^2$	2.665	367.197	2.126	8.733	0.432	0.649	10^{-5}
$\mathcal{Q}$	0.103	$< 10^{-6}$	0.119	0.003	0.511	0.421	0.998
	$\gamma_c = 1.288 \pm 0.002$	$\gamma_c = 1.076 \pm 0.001$	$\beta = 0.626 \pm 0.001$	$\gamma_c = 1.116 \pm 0.001$	$\beta = 0.878 \pm 0.001$	$\gamma_c = 0.982 \pm 0.017$	$\gamma_c = 1.002 \pm 0.018$
	$\gamma_c = \mathbf{1.271}$	$\gamma_c = \mathbf{1.004}$	$\beta = \mathbf{0.628}$	$\gamma_c = \mathbf{1.064}$	$\beta = \mathbf{0.881}$	$\gamma_c = \mathbf{0.982}$	$\gamma_c = \mathbf{1.002}$
	$\pm 0.010 \pm 0.018$	**$\pm 0.018 \pm 0.073$**	**$\pm 0.001 \pm 0.002$**	**$\pm 0.082 \pm 0.053$**	**$\pm 0.001 \pm 0.003$**	**± 0.017**	**± 0.018**

[1] E. J. Janse van Rensburg, *The Statistical Mechanics of Interacting Walks, Polygons, Animals and Vesicles* (Oxford University Press, Oxford, 2015).

[2] A. Bunde, S. Havlin, and M. Porto, Phys. Rev. Lett. **74**, 2714 (1995).

[3] M. Rubinstein and R. H. Colby, *Polymer Physics* (Oxford University Press, New York, 2003).

[4] A. R. Khokhlov and S. K. Nechaev, Phys. Lett. A **112**, 156 (1985).

[5] M. Rubinstein, Phys. Rev. Lett. **59**, 1946 (1987).

[6] S. P. Obukhov, M. Rubinstein, and T. Duke, Phys. Rev. Lett. **73**, 1263 (1994).

[7] A. Rosa and R. Everaers, Phys. Rev. Lett. **112**, 118302 (2014).

[8] A. Y. Grosberg, Soft Matter **10**, 560 (2014).

[9] J. Smrek and A. Y. Grosberg, J. Phys.: Condens. Matter **27**, 064117 (2015).

[10] T. Ge, S. Panyukov, and M. Rubinstein, Macromolecules **49**, 708 (2016).

[11] J. F. Marko and E. D. Siggia, Phys. Rev. E **52**, 2912 (1995).

[12] M. Doi and S. F. Edwards, *The Theory of Polymer Dynamics* (Oxford University Press, New York, 1986).

[13] E. J. Janse van Rensburg and N. Madras, J. Phys. A: Math. Gen. **25**, 303 (1992).

[14] B. H. Zimm and W. H. Stockmayer, J. Chem. Phys. **17**, 1301 (1949).

[15] P.-G. De Gennes, Biopolymers **6**, 715 (1968).

[16] G. Parisi and N. Sourlas, Phys. Rev. Lett. **46**, 871 (1981).

[17] H.-P. Hsu, W. Nadler, and P. Grassberger, J. Phys. A: Math. Gen. **38**, 775 (2005).

[18] A. Rosa and R. Everaers, J. Phys. A: Math. Gen. **49**, 345001 (2016).

[19] A. Rosa and R. Everaers, J. Chem. Phys. **145**, 164906 (2016).

[20] B. Derrida and L. de Seze, J. Physique **43**, 475 (1982).

[21] H.-K. Janssen and O. Stenull, Phys. Rev. E **83**, 051126 (2011).

[22] J. Isaacson and T. C. Lubensky, J. Physique Lett. **41**, 469 (1980).

[23] M. Daoud and J. F. Joanny, J. Physique **42**, 1359 (1981).

[24] A. M. Gutin, A. Y. Grosberg, and E. I. Shakhnovich, Macromolecules **26**, 1293 (1993).

[25] R. Everaers, A. Y. Grosberg, M. Rubinstein, and A. Rosa, Soft Matter (to be published).

[26] P.-G. De Gennes, *Scaling Concepts in Polymer Physics* (Cornell University Press, Ithaca, 1979).

[27] J. des Cloizeaux and G. Jannink, *Polymers in Solution* (Oxford University Press, Oxford, 1989).

[28] P. J. Flory, *Principles of Polymer Chemistry* (Cornell University Press, Ithaca, NY, 1953).

[29] A. Y. Grosberg and S. K. Nechaev, J. Phys. A-Math. Theor. **48**, 345003 (2015).

[30] A. J. Guttmann, J. Phys. A: Math. Gen. **20**, 1839 (1987).

[31] A notable exception seems to be the case of self-avoiding lattice trees (SATs). SATs are believed to fall into the same universality class as lattice animals [41,36,42] with their number scaling similarly to Eq. (14): $\mathcal{Z}_{\mathrm{SAT}}(N) \sim \mu^N N^{\gamma-1}$. In particular, the tree and animal critical exponents in d-dimensions are related to the Lee-Yang edge singularity [16,43–45] of the Ising model in an imaginary magnetic field in $(d-2)$-dimensions, suggesting a relation between the entropy and the size $\gamma(d) = 1 - \nu(d)(d-2)$. This relation implies that, at odds with the case of linear chains, it is indeed possible to estimate the number of self-avoiding trees using Flory theory.

[32] R. Everaers, I. S. Graham, and M. J. Zuckermann, J. Phys. A: Math. Gen. **28**, 1271 (1995).

[33] S. Redner, J. Phys. A: Math. Gen. **13**, 3525 (1980).

[34] M. E. Fisher, J. Chem. Phys. **44**, 616 (1966).

[35] P. Pincus, Macromolecules **9**, 386 (1976).

[36] W. A. Seitz and D. J. Klein, J. Chem. Phys. **75**, 5190 (1981).

[37] H. J. Heermann, D. C. Hong, and H. E. Stanley, J. Phys. A: Math. Gen. **17**, L261 (1984).

[38] D. Stauffer and A. Aharony, *Introduction to Percolation Theory* (Taylor & Francis Inc., London, 1994).

[39] W. H. Press, S. A. Teukolsky, W. T. Vetterling, and B. F. Flannery, *Numerical Recipes in Fortran* (Cambridge University Press, Cambridge, 1992), 2nd ed.

[40] P. Debye and F. Bueche, J. Chem. Phys. **20**, 1337 (1952).

[41] T. C. Lubensky and J. Isaacson, Phys. Rev. A **20**, 2130 (1979).

[42] J. A. M. S. Duarte and H. J. Ruskin, J. Physique **42**, 1585 (1981).

[43] M. E. Fisher, Phys. Rev. Lett. **40**, 1610 (1978).

[44] D. A. Kurtze and M. E. Fisher, Phys. Rev. B **20**, 2785 (1979).

[45] A. Bovier, J. Fröhlich, and U. Glaus, Branched polymers and dimensional reduction, in *Critical Phenomena, Random Systems, Gauge Theories*, edited by K. Osterwalder and R. Stora (North-Holland, Amsterdam, 1984).